07

Formation of GaMnAs ferromagnetic layers by implantation of Mn ions using an accelerator with a vacuum-arc source

© Yu.A. Danilov,[1] I.N. Antonov,[1] V.I. Bachurin,[2] M.V. Ved,[1] O.V. Vikhrova,[1] Yu.A. Dudin,[1] I.L. Kalentyeva,[1] R.N. Kryukov,[1] A.V. Nezhdanov,[1] A.E. Parafin,[3] S.G. Simakin,[2] P.A. Yunin[3]

[1] Lobachevsky State University,
603022 Nizhny Novgorod, Russia
[2] SRC „Kurchatov Institute" „Valiev Institute of Physics and Technology, Yaroslavl Branch,
150067 Yaroslavl, Russia
[3] Institute of Physics of Microstructures, Russian Academy of Sciences,
603950 Nizhny Novgorod, Russia
e-mail: vikhrova.olga@gmail.com

Received April 18, 2025
Revised October 23, 2025
Accepted November 26, 2025

The work is devoted to the study of the possibility of forming ferromagnetic GaMnAs layers by the manganese ion implantation method using an accelerator with a vacuum-arc source and subsequent pulsed laser annealing. It is shown that the implantation of Mn ions with doses of $2-5 \cdot 10^{16}\,cm^{-2}$ and subsequent annealing with an energy density of $\sim 300\,mJ/cm^2$ make it possible to obtain ferromagnetic semiconductor layers with a Curie temperature of up to 120 K. The manganese distribution profiles and changes in the GaAs matrix composition are studied using secondary ion mass spectrometry and X-ray photoelectron spectroscopy. The study of the optical properties of the layers, including the Raman scattering spectra, confirmed the presence of a coupled plasmon-phonon mode, which is typical for heavily doped *p*-type semiconductors. Galvanomagnetic measurements revealed an anomalous Hall effect and negative magnetoresistance at temperatures below the Curie temperature. The results show the potential of using an accelerator with a vacuum-arc ion source to create ferromagnetic semiconductor structures.

Keywords: ion implantation, pulsed laser annealing, ferromagnetism, diluted magnetic semiconductor, GaMnAs, vacuum arc accelerator.

DOI: 10.61011/TP.2026.04.63271.77-25

Introduction

Ferromagnetic semiconductors of the $A^{III}B^{V}$ type that are highly doped with Mn are promising for constructing instrument structures of spin electronics and optoelectronics. In addition to a method of low-temperature molecular-beam epitaxy, people quite often use a method of ion implantation (II) with subsequent pulsed laser annealing (PLA) [1–5]. In this respect, GaMnAs is the most studied material. We note that results obtained in several groups for implanting Mn^+ ions with energies of 50–200 keV and doses of $3-5 \cdot 10^{16}\,cm^{-2}$ into GaAs by subsequent PLA with an energy density of about $300\,mJ/cm^2$ in a nanosecond pulse are in good agreement at least with respect to a Curie temperature ($\sim 110\,K$) of produced layers [1,2,6]. The latter fact indicates well reproducibility and stability of the II+PLA technology, which can be used when implementing a process of manufacturing spintronics devices.

Usually, the Mn ions are implanted in accelerators with a gas-discharge source, in which the Mn atoms are injected when being thermally evaporated from a crucible. However, there are ion accelerators with a source based on a vacuum-arc discharge [7], when in a pulsed periodic mode a surface of a metal target is sputtered to form plasma, while a flow of the formed ions is accelerated to deliver them to an irradiated substrate. As a rule, these accelerators are used for treating metal surfaces with large ion flows, for example, for strengthening [8]. There are known russian designs of such accelerators — a series of „Raduga"units [9].

In accordance with the above said, the present study provides an investigation that confirms that it is possible to use the „Raduga-3M" vacuum-arc accelerator to produce the ferromagnetic GaMnAs layers. The applied II method makes it possible to create high intensity of the ion beam, while ensuring high doping doses due to using a solid-state cathode made of high-purity manganese. An approach considered in the present study shows versatility and relevance of using the vacuum arc accelerator within the framework of designing processes in the electronic industry.

1. Experimental procedure

The experiments were performed in the „Raduga-3M" ion accelerator. The main specific features of operation of this accelerator include [9]: first of all, the pulsed frequency-periodic mode of operation (common values of pulse current are up to 1 A, pulse duration is $\sim 200\,\mu s$ and a pulse repetition rate is up to 50 pulses/s); secondly, there is no mass separation (it means that the entire ionized beam

hits the target) and, thirdly, the ion flow contains various charge fractions. A wafer made of high-purity metallic manganese was used as a precursor in order to irradiate with the Mn ions, accelerating voltage (U) was 30 or 80 kV, the ion doses (D_i) varied from 10^{15} to $5 \cdot 10^{16}$ cm^{-2} and the target was not heated.

An original material was epi-ready wafers made of single-crystal semi-insulating gallium arsenide cut out in the plane (100).

Radiation-induced defects were removed and implanted manganese was activated using annealing by means of single pulses of an excimer KrF-laser of the LPX-200 grade. A radiation wavelength was 248 nm and pulse duration was $\sim$ 30 ns. The pulse energy density at the sample varied from 100 to 400 mJ/cm^2. The laser beam was defocused during annealing. An area of the laser beam was about 8×10 mm. At the same time, a sized of the annealed samples did not exceed 6×8 mm. They were annealed in a single pulse. The laser annealing mode used may be regarded as a liquid-phase one. Radiation of the used excimer laser is absorbed in a thin subsurface GaAs layer. At the same time, we estimate that it is possible to get to temperatures that are comparable to a melting point of GaAs (1515 K) [10].

A composition of the GaAs layers was analyzed and profiles of implanted Mn were constructed using a time-of-flight mass spectrometer TOF.SIMS5 manufactured by IONTOF GmbH, Germany (equipment belonging to Shared Use Center „Diagnostics of Micro- and Nanostructures"). At the same time, the Bi^+ ions with energy of 25 keV were used for analysis, while profiling was done by the beam of oxygen ions with energy of 1 keV. A size of an ion etching crater was typically $300 \times 300\,\mu$m, while an analysis region was $50 \times 50\,\mu$m. Depth calibration was done by measuring a crater depth in the profilometer Talystep upon termination of the etching process, so was concentration calibration using an implantation dose when taking into account ion sputtering.

The composition of the GaAs layers irradiated with the Mn ions was also studied using X-ray Photoelectron Spectroscopy (XPS). The method was based on an ultrahigh-vacuum complex Omicron Multiprobe RM. Photo-emission was excited by means of AlK$_\alpha$-radiation with energy of 1486.7 eV, and a diameter of the analysis region was 3 mm; an atomic concentration of elements was determined by a method of relative sensitivity factors. The samples were profiled by means of the beam of the Ar^+ ions (the energy is 1 keV, the current density is $0.7\,\mu$A/cm^2, the beam diameter is $\sim$ 20 mm, and the angle of inclination of the source axis to a sample normal is 45°). Since the major parameter determining depth resolution during ion etching is roughness of the surface, atomic force microscopy (AFM) was applied before and after structure profiling for monitoring a surface morphology. This method is implemented on an instrument SolverPro produced by NT-MDT (Russia). This microscope allows obtaining surface scans $50 \times 50\,\mu$m. For the experiments, we used HA_NC probes with a rounding radius below 10 nm, which are manufactured by NT-MDT. During scanning, the microscope was operated in a semi-contact mode.

The structure of the irradiated and annealed samples was studied by means of high-resolution X-ray diffractometry in a diffractometer Bruker D8 Discover (equipment belonging to Shared Use Center „Physics and Technology of Micro- and Nanostructures" of the IAP RAS). $\omega/2\theta$-scans were shot with a double-reflection monochromator Ge(220) (CuK$_{\alpha 1}$-line of radiation, $\lambda = 1.54056$ A) on a primary beam. Obtained diffraction patterns were processed in a DIFFRAC.Leptos software package by calculating and fitting model curves using a dynamic diffraction theory. Variable parameters of the model included a thickness of the deformed layer and a strain value that can be lately recalculated into the manganese concentration.

GaMnAs reflection spectra were studied at the room temperature by means of a Varian Cary 6000i spectrophotometer within a light quantum energy range 1.5–6.0 eV; at the same time an attachment for reflection at the angle of 12.5° to the normal was used.

Raman scattering (RS) was studied using an NTEGRA Spectra complex and it also used a laser with the radiation wavelength of 473 nm and power of 0.5 mW. The measurement range was 50–900 cm^{-1} with resolution of 0.7 cm^{-1}. Back-scattering geometry was used, while the measurements were at the room temperature. The exposure time during measurements was 120 s.

The galvanomagnetic measurements were done using a measuring complex that included a Keithley 2400 source meter and a closed-type helium cryostat Janis CCS-300S/202. A measurement temperature varied from 10 to 300 K, while a range of magnetic fields was usually ±3600 Oe.

2. Experimental results

2.1. Composition and structure of GaAs irradiated with Mn ions

Fig. 1 shows the manganese-doped profiles that are obtained by Secondary Ion Mass Spectrometry (SIMS) for the sample with implantation at accelerating voltage of $U = 80$ kV and the dose of $3 \cdot 10^{15}$ cm^{-2}.

The curve *1* is a profile calculated by means of the SRIM-2013 software [11]; it took into account that the ion beam hitting the irradiated wafer was a multi-energy one. The literature contains no data about the composition of the beam of the manganese ions in the accelerator of the „Raduga-3M" type. Therefore, values of the composition of the charge fractions in the vacuum-arc discharge source were used from [7]: 49 % of the Mn^+ ions, 50 % of Mn^{2+} and 1 % of Mn^{3+}. We have separately calculated for GaAs implantation of the ions with energy of 80, 160 and 240 keV according to a charge value and then summed taking into account the composition of the charge fractions. Besides, similar to the study [12], we took into account ion sputtering during irradiation: a sputtering ratio calculated in

the SRIM software taking into account charge fractioning was $S = 8.10$ at./ion.

The curve *2* of Fig. 1 is an experimental profile for implantation of Mn with $U = 80$ kV and the dose of $D_i = 3 \cdot 10^{15}$ cm^{-2} without annealing. Note that the profile is „pulled" to the surface with considerable increase of the concentration of the Mn atoms in the layer of the thickness of ~ 40 nm. One can notice a local maximum near the surface at the depth about 15 nm; this magnitude of an average projected flight is matched with 20 keV-energy of the Mn ions. The observed significant divergence between the value of 20 keV and specified $U = 80$ kV states against „energy" explanation of difference of the experimental and calculated profile of the Mn atoms. Possible causes of the divergence will be discussed below in Section 3.

The curve *3* (Fig. 1) shows the experimental SIMS profile of the Mn atoms after laser annealing with the pulse energy density of $P = 400$ mJ/cm^2. Near the surface down to the depth of ~ 50 nm, this profile does not greatly differ from the profile just after implantation (the curve *2*). The depth range from 50 to 130 nm exhibits a „tail", which can be related to diffusion of the Mn atoms during annealing. But a concentration level in this range is not high ($< 10^{20}$ cm^{-3}).

The SIMS-profiling method was used to obtain distributions of components of a GaAs matrix along the depth of the layer irradiated with the Mn ions, as well. It turned out that after irradiation with $U = 80$ kV and $D_i = 3 \cdot 10^{15}$ cm^{-2} the Ga content was equal to a volume one ($x_{\text{Ga}} = 0.5$) across the entire irradiated layer, while starting from the depths ~ 160 nm the As content decreases towards the surface down to $x_{\text{As}} \sim 0.45$. As a result of laser annealing ($P = 400$ mJ/cm^2) the distributions of the elements had somewhat changed: the As content is approximately equal to a stoichiometric one from the substrate up to ~ 60 nm and decreases towards the surface down to the value ~ 0.45; the Ga content differs from the stoichiometric only within the range 80–180 nm ($x_{\text{Ga}} \sim 0.49$), which can be related to activation (embedment into a Ga sublattice) of implanted Mn.

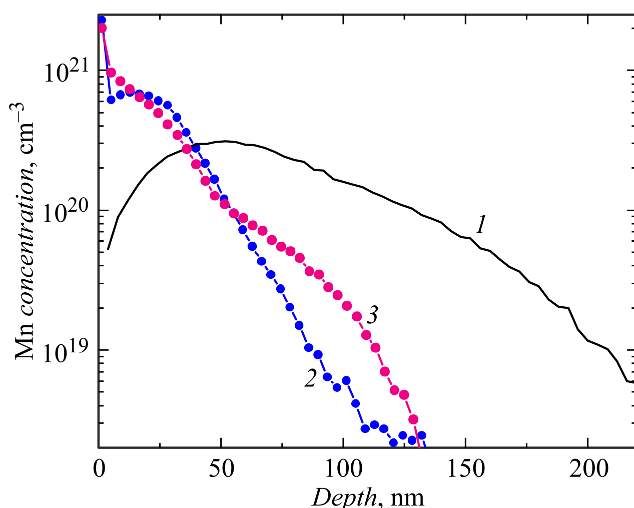

Figure 1. Profiles of Mn atoms implanted into GaAs with accelerating voltage of 80 kV and a dose of $3 \cdot 10^{15}$ cm^{-2}: *1* — calculated by means of the SRIM software; *2* — SIMS-profile after implantation; *3* — SIMS-profile after implantation and PLA with the energy density of 400 mJ/cm^2.

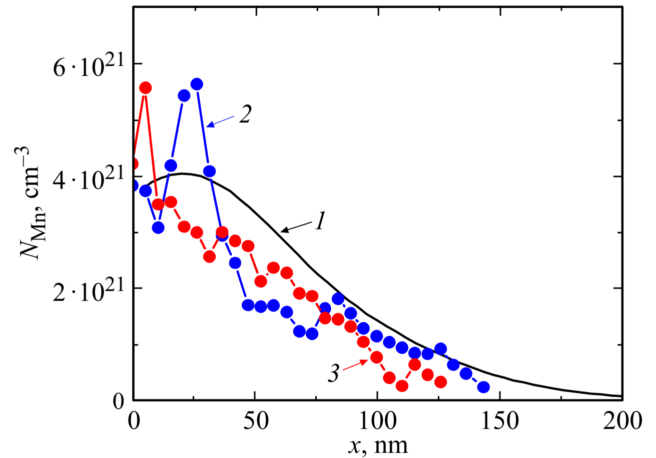

Figure 2. Profiles of Mn distributions in GaAs as a result of implantation with $U = 80$ kV, $D_i = 5 \cdot 10^{16}$ cm^{-2}: *1* — SRIM calculation with taking into account sputtering; *2* — XPS profile after implantation; *3* — XPS profile after implantation and PLA with $P = 400$ mJ/cm^2.

The composition of GaAs irradiated with higher Mn doses has been profiled by X-ray Photoelectron Spectroscopy.

Fig. 2 shows the profiles obtained by the XPS method for the samples irradiated with the manganese ions with accelerating voltage of 80 kV and the dose of $5 \cdot 10^{16}$ cm^{-2}. The curve *1* shows the calculates SRIM profile with taking into account sputtering. We note that as expected when taking into account ion sputtering [13], the calculated maximum of distribution of the Mn atoms ($x_m \sim 20$ nm) is closer to the surface than a peak ($x_m = 52$ nm) directly obtained from the SRIM calculation (without taking into account ion sputtering). At the same time, the calculated concentration of the Mn atoms in the distribution maximum also decreases from $5.2 \cdot 10^{21}$ to $\sim 4 \cdot 10^{21}$ cm^{-3} when taking into account ion sputtering. The profile *1* was integrated to calculate a post-sputtering dose of the Mn atoms (D_r), which was $D_r = 3.47 \cdot 10^{16}$ cm^{-2} for the above-said conditions.

The curve *2* of Fig. 2 is a profile that is experimentally obtained by the XPS method with layer-by-layer etching for the implanted (without annealing) sample. We indicate that the concentrations of the Mn atoms well agree with the calculated profile within a section from 80 to 140 nm. Near the surface (from 15 to 30 nm), we observe an excess of the concentration of the Mn atoms above the calculations (above an error of ~ 1% for determining N_{Mn} using the method of relative sensitivity factors) apparently due to depletion of surrounding layers. The curve *2* is integrated to provide a value of $2.92 \cdot 10^{16}$ cm^{-2}, which

is an experimental magnitude of D_r. This magnitude is by $\sim 15\,\%$ smaller than the calculated one; the divergence may be related to the fact that the XPS profiling method included depth calibration by a measured rate of ion etching of GaAs, while in case of GaAs irradiated with the Mn ions the etching rate can vary. It should be underlined that in the XPS method calibration by the Mn concentration (the procedure of relative sensitivity factors) does not depend on the II conditions unlike calibration in the SIMS method (Fig. 1), which uses the calculated value of D_r. Therefore, as a whole it can be stated that the calculation taking into account a multi-energy factor and ion sputtering on the one hand and XPS profiling on the other provide satisfactory agreement in terms of the residual dose of implantation.

XPS profiling of the sample produced by radiation with the Mn ions with accelerating voltage of 30 kV and the dose of $D_i = 5 \cdot 10^{16}\,\mathrm{cm}^{-2}$ (the profile is not shown) has specific features that are similar to the profile for the implanted sample with $U = 80\,\mathrm{kV}$: the concentration of the Mn atoms is somewhat higher than the calculated one within the depth range from 15 to 35 nm and drops to zero almost like the calculated one at the depth near 50 nm. At the same time, the experimental value of the residual dose is $1.85 \cdot 10^{16}\,\mathrm{cm}^{-2}$, which does not greatly differ from the calculated value $D_r = 1.72 \cdot 10^{16}\,\mathrm{cm}^{-2}$. The significant increase of the ion-sputtered dose of the Mn atoms ($D_i - D_r = 3.28 \cdot 10^{16}\,\mathrm{cm}^{-2}$) in case of $U = 30\,\mathrm{kV}$ as compared to the sample for $U = 80\,\mathrm{kV}$ ($D_i - D_r = 1.53 \cdot 10^{16}\,\mathrm{cm}^{-2}$) is explained both by a smaller flight of the Mn ions as well as the increase of the ion sputtering ratio to $S = 9.48$ at./ion at the lower ion energy.

The curve *3* of Fig. 2 shows the distribution of the concentration of the Mn atoms along the GaAs depth after irradiation with $U = 80\,\mathrm{kV}$, $D_i = 5 \cdot 10^{16}\,\mathrm{cm}^{-2}$ and PLA with $P = 400\,\mathrm{mJ/cm}^2$. It is clear that the concentration of the Mn atoms across the entire doped layer is less than the calculated values approximately by $0.5{-}1 \cdot 10^{21}\,\mathrm{cm}^{-3}$, while the peak is shifted into the subsurface region of the depth of 10 nm. At the same time, the experimental residual dose is $D_r = 2.64 \cdot 10^{16}\,\mathrm{cm}^{-2}$, i.e. as a result of annealing another $\sim 10\,\%$ of the Mn atoms is lost in total. Formation of the manganese-enriched surface layer during PLA has been previously noted [2] and the phenomenon is related by the authors to segregation of the Mn atoms when a recrystallization front moves to the surface during cooling upon termination of the leaser pulse.

It can be noted that Mn implantation and PLA resulted in a slight increase of roughness of the GaAs surface: the RMS value has changed from 0.4 nm for the original sample to 2.5 nm for the sample after implantation with $D_i = 5 \cdot 10^{16}\,\mathrm{cm}^{-2}$ and annealing with $P = 400\,\mathrm{mJ/cm}^2$. Layer-by-layer etching of the samples by irradiating with the low-energy Ar^+ ions neither caused noticeable changes in the morphology, thereby meaning insignificant variation of the error in profiling the doped layers.

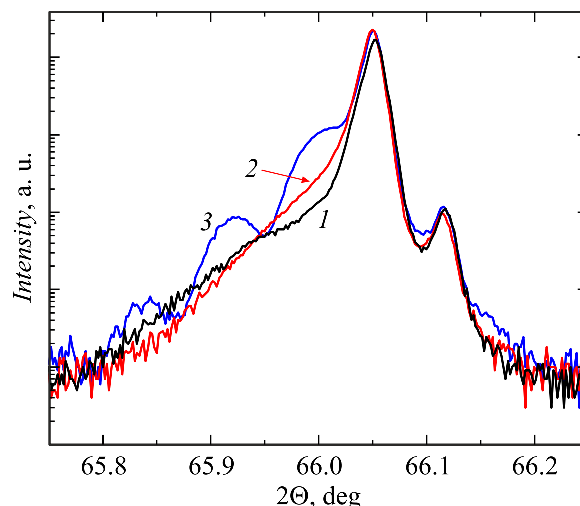

Figure 3. X-ray diffraction patterns of the GaMnAs samples produced by implantation of ions with accelerating voltage of 80 kV, of the dose of $5 \cdot 10^{16}\,\mathrm{cm}^{-2}$ and subsequent PLA with the various energy density, mJ/cm^2: *1* — 200, *2* — 300, *3* — 400.

The distribution of the components of the GaAs matrix is also interesting. For the manganese-irradiated sample ($U = 30\,\mathrm{kV}$, $D_i = 5 \cdot 10^{16}\,\mathrm{cm}^{-2}$), the entire range of the doping depths (0–50 nm) exhibits shortage of the Ga atoms as compared to As with the highest difference ~ 12 at.% around the Mn distribution maximum. Similarly, the irradiated (without PLA) sample with $U = 80\,\mathrm{kV}$, $D_i = 5 \cdot 10^{16}\,\mathrm{cm}^{-2}$ also exhibits Ga shortage across the entire doped layer (0–145 nm) with the highest difference ~ 5 at.% around the Mn concentration maximum (the depths 15–35 nm). The situation substantially changes after PLA: for the sample ($U = 80\,\mathrm{kV}$, $D_i = 5 \cdot 10^{16}\,\mathrm{cm}^{-2}$, $P = 400\,\mathrm{mJ/cm}^2$) the subsurface layer 0–30 nm exhibits As shortage (the maximum at 5 at.%), while the depth range 50–125 nm is dominated by As with the difference of up to 2–3 at.%. Probably, this range is matched with a location of electrically-active manganese, i.e. Mn_{Ga}. Based on the XPS results, a state of the embedded manganese impurity was analyzed according to a previously developed procedure [14]. According to this analysis, the high portion of manganese is embedded into the gallium sublattice to substitute it (manganese is an acceptor). Besides, a part of the impurity occupies an interstitial position and becomes a donor. Moreover, manganese on the structure surface and nearby forms oxygen compounds that are not electrically-active.

Fig. 3 shows the curves of X-ray diffraction reflection of the GaMnAs samples after implantation with $U = 80\,\mathrm{kV}$, of the dose $5 \cdot 10^{16}\,\mathrm{cm}^{-2}$ and PLA with varying the density of the laser pulse energy.

A type of the curves indicates a deformed layer, apparently, of GaMnAs, with a lattice parameter (a_{GaMnAs}) that exceeds a lattice parameter of the GaAs substrate ($a_{\mathrm{GaAs}} = 0.5653\,\mathrm{nm}$). The magnitude a_{GaMnAs} slightly

varied when the PLA energy density was varied within the range 200–400 mJ/cm^2, but it depended on the ion dose: at the dose of $1 \cdot 10^{16}$ cm^{-2} the value of $a_{\text{GaMnAs}} = 0.5654$ nm; at the dose of $5 \cdot 10^{16}$ cm^{-2} $a_{\text{GaMnAs}} = 0.5657$ nm. It should be noted that the increase of PLA power results in a decrease of a width of the X-ray diffraction peak of the deformed layer. The thickness is estimated by modeling and curve fitting to be 50, 80 and 165 nm for the values $P = 200$, 300 and 400 mJ/cm^2, respectively. Presumably, the increase of PLA power results in recrystallization of a larger thickness of the implanted layer and introduction of Mn as a „structure" impurity for a larger depth, accordingly. Presence of oscillations of a thickness contrast for PLA with $P = 400$ mJ/cm^2 indicates formation of the layer with relatively homogeneous distribution of strain along the thickness and a quite sharp boundary with the undeformed substrate. It should be noted that when $2\theta \sim 66.12°$ the right side of the substrate peak exhibits a peak that is an artefact of measurement in this diagram with the double-reflection monochromator (reflection of the CuK$_{\alpha 2}$-line for the GaAs substrate).

2.2. Optical properties

Studies of the spectral dependence of the reflection coefficient R can carry information on changes of a band structure of the semiconductor [15]. In Fig. 4, the curve *1* shows a dependence of R on light quantum energy E for single-crystal i-GaAs(001). Three peaks are clearly discerned (which are marked with vertical lines): a doublet when $E = 2.90$ and 3.12 eV and a peak at 5.08 eV, which

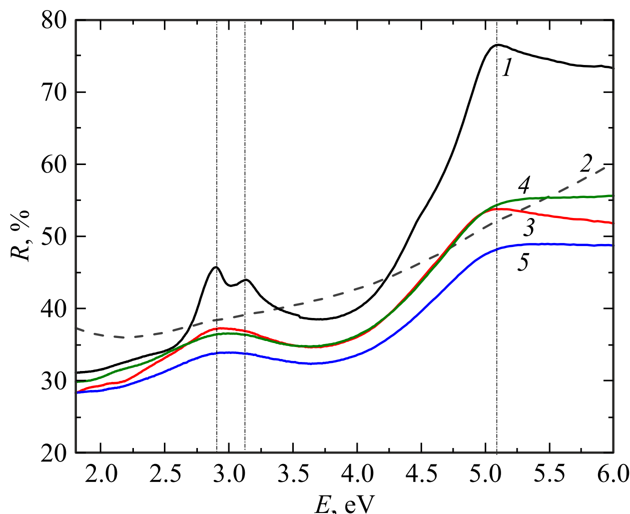

Figure 4. Spectral dependences of the reflection coefficient of single-crystal GaAs (the spectrum *1*) and GaAs irradiated with the Mn ions (accelerating voltage = 80 kV, the dose is $1 \cdot 10^{16}$ cm^{-2}) (the spectrum *2*). The reflection spectra of the samples irradiated with Mn with the various dose, after PLA with the energy density of 400 mJ/cm^2: the spectrum *3* corresponds to the dose of $1 \cdot 10^{16}$ cm^{-2}, the spectrum *4* to the dose of $3 \cdot 10^{16}$ cm^{-2} and the spectrum *5* to the dose of $5 \cdot 10^{16}$ cm^{-2}.

correspond to interband transitions of the type E_1 and $E_1 + \Delta$ and E_2 [13].

As a result of implantation of the Mn ions with the dose of $1 \cdot 10^{16}$ cm^{-2}, the spectrum was structureless (the curve *2*), thereby indicating full disordering of the subsurface layer that forms a reflected signal. With the manganese ions' dose of $D = 1 \cdot 10^{16}$ cm^{-2}, the annealing pulse energy's density of 200 mJ/cm^2 is enough for restoring a crystal structure: the spectrum R (not shown) is generally similar to a spectrum of single-crystal GaAs. But instead of the doublet E_1 and $E_1 + \Delta$ a quite wide peak appears (the doublet is not resolved, since edges of the Brillouin zone are smeared due to heavy GaAs doping), while the peak E_2 at ~ 5 eV is well visible. When the pulse energy is 300 and 400 mJ/cm^2, the spectrum (the curve *3*) is almost unchanged within the transitions E_1 and $E_1 + \Delta$ as compared to the sample annealed at 200 mJ/cm^2. The reflection peak slightly increases at ~ 5 eV and has almost no change in its form.

It is clear from Fig. 4 that for the doses $3 \cdot 10^{16}$ and $5 \cdot 10^{16}$ cm^{-2} the structure is restored less efficiently. Although the wide peak corresponding to the transitions E_1 and $E_1 + \Delta$ already appears when the annealing pulse energy is 200 mJ/cm^2, but even after annealing at $P = 400$ mJ/cm^2 (the curves *4* and *5* in Fig. 4) a height of the peaks does not reach a height of the peaks for the ions dose of $1 \cdot 10^{16}$ cm^{-2}. Besides, the peak near the values ~ 5 eV is inexplicit (it is seen as a shoulder).

Below are results of investigation of the RS spectra of the GaAs samples that are irradiated with the Mn ions in the various process modes of layer formation. Fig. 5, *a* shows the RS spectra of the GaAs sample with implanted Mn (the ions' dose is $1 \cdot 10^{16}$ cm^{-2}) before laser annealing.

It is clear that even at this dose implantation of the ions results in heavy lattice disturbance as an appearing wide band of the RS signal, which is radically different from the spectrum for crystalline GaAs. Taking into account the results of investigation of the reflection spectra (Fig. 4, the curve *2*), we can assert that implantation of the Mn ions included full disordering of the subsurface layer due to appearance of the radiation-induced defects. It necessitates application of annealing for crystallization of the layers of GaAs irradiated with the Mn ions.

After laser annealing with $P = 200$ mJ/cm^2 the RS spectrum is substantially changed (Fig. 5, *a*, the curve *2*): at the wave number of 290 cm^{-1} a narrow peak appears and it corresponds to an LO phonon of crystalline GaAs [16]. It explicitly indicates recrystallization of GaAs irradiated by the manganese ions, as a result of PLA. Nevertheless, the RS spectrum of the annealed GaMnAs sample includes the most intense line at ~ 265 cm^{-1}, which corresponds to the coupled phonon-plasmon mode (CPPM) as per [17,18]. Presence of this peak indicates electrical activation of the impurity in gallium arsenide.

With an increase of the implantation dose, the CPPM position (Fig. 5, *b*) is shifted towards the smaller wave numbers, while intensity of the LO mode of GaAs monotonously

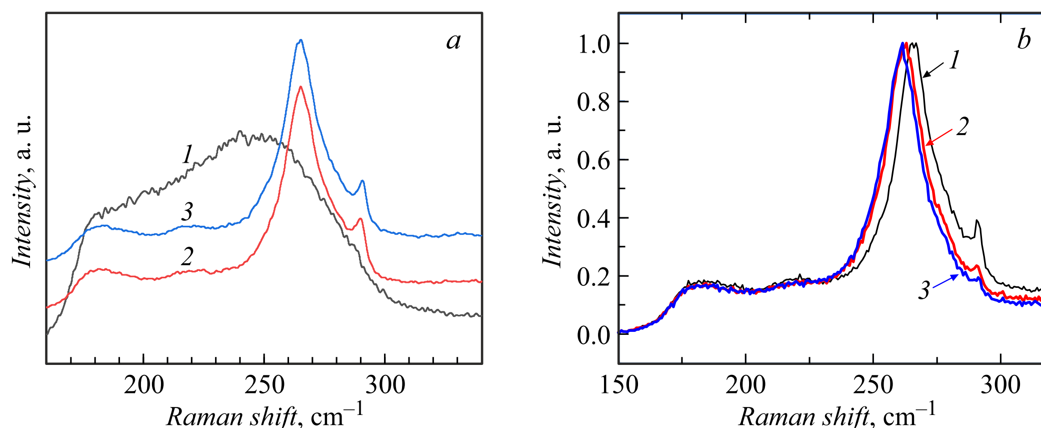

Figure 5. RS spectra of the samples irradiated with the Mn ions when $U = 80$ kV: *a* — $D_i = 1 \cdot 10^{16}$ cm^{-2}, before (the curve *1*) and after laser annealing with $P = 200$ (the curve *2*) and 300 mJ/cm^2 (the curve *3*); *b* — annealing with $P = 400$ mJ/cm^2 at the various doses of implantation. Numbers of the curves correspond to the doses: *1* — $1 \cdot 10^{16}$, *2* — $3 \cdot 10^{16}$, *3* — $5 \cdot 10^{16}$ cm^{-2}.

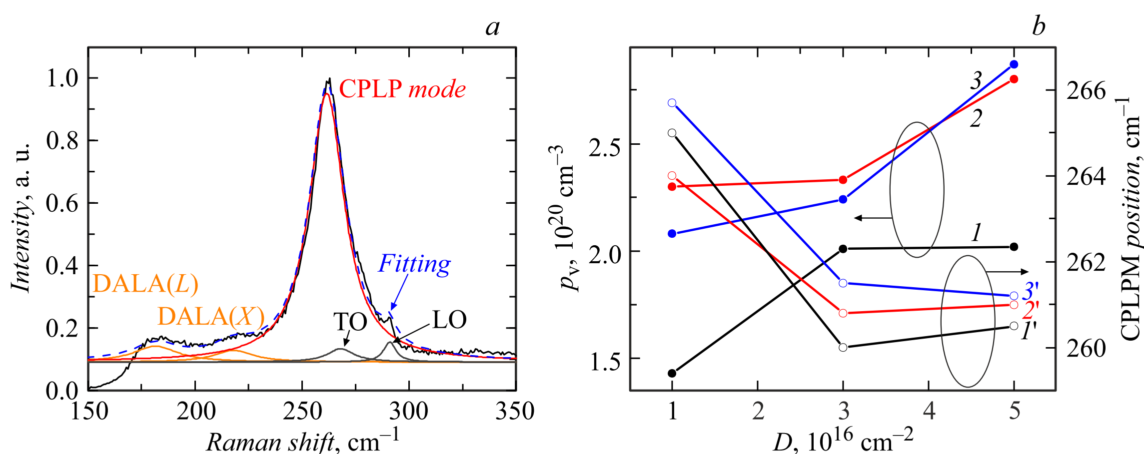

Figure 6. *a* — Lorentzian fitting of the RS spectrum for the GaMnAs sample ($U = 80$ kV, $D_i = 3 \cdot 10^{16}$ cm^{-2}, $P = 400$ mJ/cm^2); *b* — dose dependences of the hole concentration (*1–3*) and positions of the coupled phonon-plasmon mode (*1'–3'*) when varying the laser annealing energy density, mJ/cm^2: *1*, *1'* — 200; *2*, *2'* — 300; *3*, *3'* — 400.

decreases. So for the sample irradiated by Mn with the dose of $5 \cdot 10^{16}$ cm^{-2} this peak is almost indistinguishable from a background component.

The RS spectra were approximated by summing the Lorentzians, whereas each of them corresponds to a certain phonon mode. Fig. 6, *a* shows the RS spectrum for the sample irradiated at $U = 80$ kV, $D_i = 3 \cdot 10^{16}$ cm^{-2} and annealed at $P = 400$ mJ/cm^2 and expansion of the spectrum with the Lorentzians. The position of the TO- and LO-modes of GaAs complies with literature data for crystalline GaAs (269 and 291 cm^{-1} , respectively) [16]. The spectra were approximated to ascertain that in addition to the above-said shift of the CPPM maximum the growth of the dose of the Mn ions also includes a growth of its width, while an increase of pulse energy results in an increase of CPPM intensity,which is due to better activation of the impurity during annealing.

Changes of the CPPM position of the GaMnAs samples, which are associated with respective doses of the ions, are shown in Fig. 6, *b* (the curves *1'–3'*). Origin of the intense peak in the RS spectra of the ion-implanted and annealed samples as a CPPM is also proven by explicit correlation of its shift towards the smaller wave numbers with the increase of the hole concentration (the curves *1–3*) in the layer (see Section 2.3).

2.3. Galvanomagnetic properties of GaMnAs

After II (without annealing) the electrical properties of the GaAs layers are determined by presence of the radiation-induced defects. Thus, for the samples irradiated with the dose of $1 \cdot 10^{16}$ cm^{-2} ($U = 80$ kV) layer resistance was $1.29 \cdot 10^5\ \Omega/\square$ (reliability of this value is determined by a lack of shunting action of the semi-insulating substrate, for which $R_S \sim 10^9\ \Omega/\square$). At the same time, the conductivity

Table 1. Layer electrical parameters of the GaMnAs samples produced when varying the implantation dose D_i and the laser annealing energy P. Accelerating voltage $U = 80$ kV. Measurement temperature = 300 K

Layer resistance R_S, Ω/□			
P, mJ/cm^2	D_i, cm^{-2}		
	$1 \cdot 10^{16}$	$3 \cdot 10^{16}$	$5 \cdot 10^{16}$
100	1450	950	1060
200	655	525	475
300	540	435	420
400	575	440	455
Effective Hall mobility μ_{eff}, cm^2/(V·s)			
P, mJ/cm^2	D_i, cm^{-2}		
	$1 \cdot 10^{16}$	$3 \cdot 10^{16}$	$5 \cdot 10^{16}$
100	6.9	6.8	5.7
200	6.7	5.9	6.5
300	5.0	6.2	5.3
400	5.2	6.4	4.8
Layer hole concentration p_s, cm^{-2}			
P, mJ/cm^2	D_i, cm^{-2}		
	$1 \cdot 10^{16}$	$3 \cdot 10^{16}$	$5 \cdot 10^{16}$
100	$6.25 \cdot 10^{14}$	$9.66 \cdot 10^{14}$	$1.04 \cdot 10^{15}$
200	$1.43 \cdot 10^{15}$	$2.01 \cdot 10^{15}$	$2.03 \cdot 10^{15}$
300	$2.30 \cdot 10^{15}$	$2.33 \cdot 10^{15}$	$2.81 \cdot 10^{15}$
400	$2.08 \cdot 10^{15}$	$2.24 \cdot 10^{15}$	$2.87 \cdot 10^{15}$

type is electronic and a mobility value of the carriers is 0.4 cm^2/(V·s), which clearly indicates hopping conductivity across the defects.

After implantation of the Mn ions and laser annealing, the Hall effect at the room temperature is linear for all the studies samples, i.e. a Hall difference of potentials is proportional to strength of the magnetic field (H). Therefore, the measurements at $T_m = 300$ K were done at a fixed value $H = 5500$ Oe (the Nanometrics HL5500 unit). Table 1 shows the layer Hall parameters for the samples produced when varying the implantation dose within the range $1-5 \cdot 10^{16}$ cm^{-2} and the laser annealing energy within the range 100−400 mJ/cm^2. All the studied samples produced in the said modes indicate the p-type of conductivity.

We note the following trends in variation of the layer parameters of the samples when varying the modes of implantation and annealing. First of all, the layer hole concentration monotonically increases with the increase of the implantation dose at all the laser annealing energies used and reaches the maximum value $\sim 3 \cdot 10^{15}$ cm^{-2}. It corresponds to a free carriers' average concentration of $2.4 \cdot 10^{20}$ cm^{-3}, if we assume that the full thickness of the alloyed layer is ~ 125 nm according to Fig. 2. The Hall mobility 5−7 cm^2/(V·s) noticeably exceeds the values that are typical for hopping conductivity (< 1 cm^2/(V·s)) and reflects the quite high concentration of the ionized scattering centers (Mn_{Ga}). Secondly, the minimum values of layer resistance are obtained when $P = 300$ mJ/cm^2 and this magnitude may be assumed to be an optimal value of the annealing pulse energy density.

Table 2. Layer electrical parameters of the GaMnAs samples produced when $U = 30$ kV, $D_i = 2 \cdot 10^{16}$ cm^{-2}, at the various laser annealing energies P. Measurement temperature = 300 K

P, mJ/cm^2	Layer resistance R_S, Ω/□	Effective Hall mobility μ_{eff}, cm^2/V·s	Layer concentration of holes p_s, cm^{-2}
200	660	6.9	$1.36 \cdot 10^{15}$
250	530	4.7	$2.51 \cdot 10^{15}$
300	520	3.8	$3.15 \cdot 10^{15}$

The said trends of variation of the electrical properties are also kept during implantation of the Mn ions with acceleration voltage of 30 kV. Table 2 shows the Hall parameters for the GaMnAs samples produced when $U = 30$ kV, $D_i = 2 \cdot 10^{16}$ cm^{-2}, after laser annealing with $P = 200-300$ mJ/cm^2.

The p-type of conductivity stably appears as well. As a whole, the electrical parameters of the layer are close to the parameters for implantation with $U = 80$ kV; we just note somewhat smaller mobility of holes and higher layer resistance at the similar modes of implantation and annealing, which can be quite reasonably explained by the thinner doped layer when $U = 30$ kV.

We also indicate another specific feature of the GaMnAs layers produced by II and PLA: quite high stability of the electrical parameters when the samples are stored. In particular, for the layers produced when $U = 80$ kV, $D_i = 3 \cdot 10^{16}$ cm^{-2} and $P = 300$ mJ/cm^2, after storage during 965 days at 300 K in air the change of the parameters was the least: the value of R_S changes from the initial magnitude of 434 to 439 Ω/□; mobility changed from 6.2 to 6.6 cm^2/(V·s), so did the layer concentration — from $2.30 \cdot 10^{15}$ to $2.15 \cdot 10^{15}$ cm^{-2}.

When the measurement temperature is reduced (T_m) from the room temperature to 10 K, the electrical properties of the ion-implanted and annealed layers noticeably change. Fig. 7 shows dependences of resistance of the layers on T_m for the two GaMnAs samples.

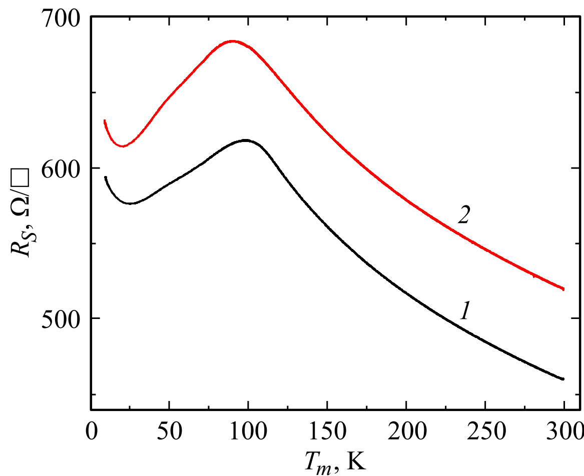

Figure 7. Dependence of resistance of the GaMnAs layers on the measurement temperature: *1* — the sample is produced when $U = 80\,\text{kV}$, $D_i = 5 \cdot 10^{16}\,\text{cm}^{-2}$, $P = 400\,\text{mJ/cm}^2$; *2* — when $U = 30\,\text{kV}$, $D_i = 2 \cdot 10^{16}\,\text{cm}^{-2}$, $P = 350\,\text{mJ/cm}^2$.

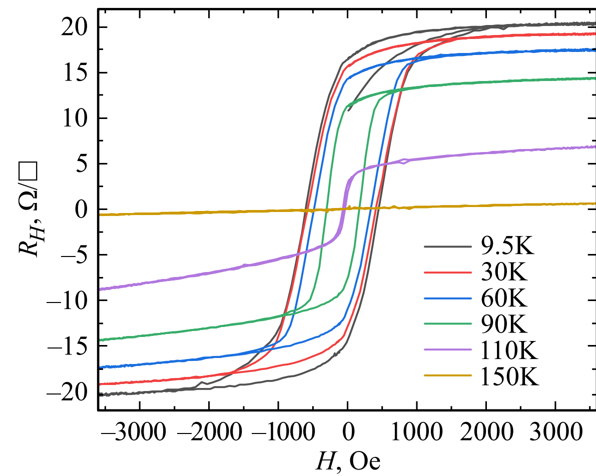

Figure 8. Magnetic-field dependences of Hall resistance when varying the measurement temperature for the GaMnAs sample produced by implantation of the ions when $U = 80\,\text{kV}$, $D_i = 3 \cdot 10^{16}\,\text{cm}^{-2}$ and PLA when $P = 300\,\text{mJ/cm}^2$.

We observe appearance of resistance maximums that are typical for the ferromagnetic semiconductors: at 99 K for the modes of production $U = 80\,\text{kV}$, $D_i = 5 \cdot 10^{16}\,\text{cm}^{-2}$, $P = 400\,\text{mJ/cm}^2$ and at 89 K for the sample with $U = 30\,\text{kV}$, $D_i = 2 \cdot 10^{16}\,\text{cm}^{-2}$, $P = 350\,\text{mJ/cm}^2$. The positions of these maximums usually serve as an approximate estimation of the values of the Curie temperature.

When the measurement temperature is reduced to values of about the positions of the maximums of $R(T_m)$ or below, the Hall effect becomes anomalous, i.e. the dependence of Hall resistance on the magnetic field exhibits nonlinearity. It is typical that a hysteresis loop appears on the dependences $R_H(H)$. Fig. 8 shows the magnetic-field dependences of Hall resistance for the GaMnAs sample produced when implanting the Mn ions with $U = 80\,\text{kV}$, $D_i = 3 \cdot 10^{16}\,\text{cm}^{-2}$, after laser annealing with the energy density of $300\,\text{mJ/cm}^2$.

Starting from the temperature of 9.5 K, the hysteresis loop is monotonously narrowed, while an anomaly in the Hall effect is kept up to 110 K. The temperature dependences of the value of a coercive field for this studied mode of formation of the GaMnAs layers and some others are shown in Fig. 9.

By taking into account the results of studies of the Hall effect, we can say that the GaMnAs layers formed by implantation of the ions in the vacuum-arc accelerator are ferromagnetic semiconductors at the irradiation doses $2{-}5 \cdot 10^{16}\,\text{cm}^{-2}$ after annealing by the excimer laser pulse with the energy density $250{-}400\,\text{mJ/cm}^2$ both at accelerating voltage of 80 kV and when $U = 30\,\text{kV}$ as well.

This statement is also supported by measurements of magnetoresistance ($\text{MR} = (R_H - R_0)/R_0$, where R_H is resistance when applying the field H, while R_0 is resistance without the magnetic field) in the dependence on strength of the magnetic field. As an example, Fig. 10 shows

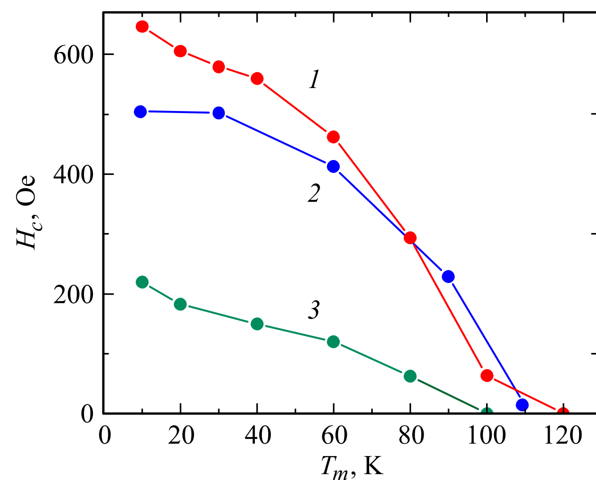

Figure 9. Dependences of the coercive field, which are obtained based on the magnetic-field curves $R_H(H)$ for the following modes of production of the GaMnAs layers: *1* — $U = 80\,\text{kV}$, $D_i = 5 \cdot 10^{16}\,\text{cm}^{-2}$, $P = 400\,\text{mJ/cm}^2$; *2* — $U = 80\,\text{kV}$, $D_i = 3 \cdot 10^{16}\,\text{cm}^{-2}$, $P = 300\,\text{mJ/cm}^2$; *3* — $U = 30\,\text{kV}$, $D_i = 2 \cdot 10^{16}\,\text{cm}^{-2}$, $P = 250\,\text{mJ/cm}^2$.

the magnetic-field dependences of magnetoresistance of the GaMnAs sample after implantation of the ions with $U = 30\,\text{kV}$, $D_i = 2 \cdot 10^{16}\,\text{cm}^{-2}$ and laser annealing with $P = 350\,\text{mJ/cm}^2$ when varying the measurement temperature. The general trend is that magnetoresistance is negative and it is related to an increase of mobility of free holes when aligning magnetic moments of the Mn atoms by the external magnetic field. At the low temperatures, we observe highly-pronounced portions of anisotropic magnetoresistance, whose contribution to the whole MR decreases as T_m increases.

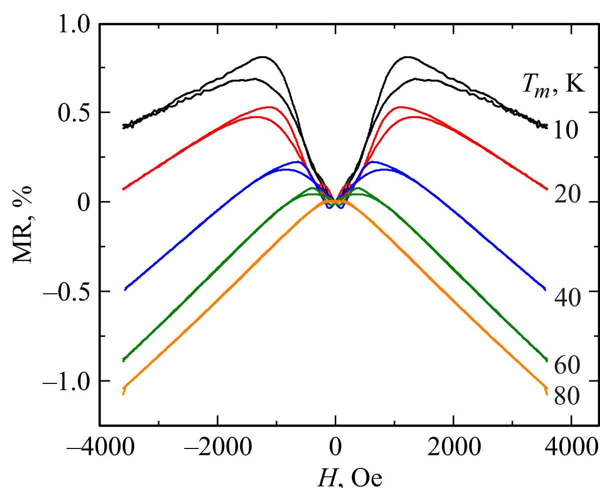

Figure 10. Magnetoresistance of the GaMnAs sample after implantation of the ions with $U = 30\,\text{kV}$, $D_i = 2 \cdot 10^{16}\,\text{cm}^{-2}$ and laser annealing with $P = 350\,\text{mJ/cm}^2$. The magnetic field is applied perpendicular to the sample plane.

3. Discussion of results

In view of objectives of the present study, it makes sense to compare the properties of the GaMnAs layers produced in the performed investigation with properties of the layers produced by monoenergetic II in the accelerator with mass separation with subsequent PLA. An object of comparison was the study [12], which describes properties of layers produced during implantation of the Mn ions into GaAs that had the energy of 180 kV, which is close to160 keV — the energy value for a prevalent fraction of the manganese ions in the vacuum-arc accelerator (Mn^{++} when $U = 80\,\text{kV}$).

Firstly, we note that after monoenergetic implantation of the ions Mn^+ (without PLA) the profile of the manganese atoms almost coincides with the calculated (SRIM) profile that takes into account ion sputtering (the curves *1* and *2* in Fig. 1 of the study [12]). In case of implantation in the „Raduga-3M“ accelerator, the implantation profile noticeable differs from the calculated one (Fig. 2, the curves *1* and *2* of the present study): we observe redistribution of the Mn atoms towards the surface with formation of a maximum in the layer of the depth 15–30 nm. The similar behavior (redistribution of manganese towards the surface as compared to the calculated profile) is also noted for other conditions of implantation in the „Raduga-3M“ ($U = 80\,\text{kV}$, $D_i = 3 \cdot 10^{15}\,\text{cm}^{-2}$ (Fig. 1, the curves *1* and *2*); $U = 30\,\text{kV}$, $D_i = 5 \cdot 10^{16}\,\text{cm}^{-2}$ is an experimental profile described in Section 2.1). We believe that the detected specific feature of the profiles of distribution of implanted (without annealing) Mn is related to a high-current pulsed nature of irradiation in the vacuum-arc accelerator. During the ion pulse of duration $\sim 200\,\mu\text{s}$, a sample area with release of energy transferred by the ions to a phonon subsystem of the semiconductor is heated and when a temperature front moves to the surface during cooling upon termination of the pulse the manganese atoms segregate towards the surface like it happens during pulsed laser annealing [2]. It is known that a phenomenon of heating by the intense ion beam is used for annealing amorphous layers of semiconductors [19].

As in case with monoenergetic implantation of the ions Mn^+ [12], PLA results in redistribution of the manganese atoms towards the surface (Fig. 2, the curve *3*). At the same time, surfaced manganese is electrically-inactive, since it reacts with oxygen in an atmosphere, in which the sample is stored. Presence of a high amount of oxygen (≥ 10 at.%) was recorded by us by the XPS method in the layer of the depth 0–10 nm from the surface for the sample with the conditions of production $U = 80\,\text{kV}$, $D_i = 5 \cdot 10^{16}\,\text{cm}^{-2}$, $P = 400\,\text{mJ/cm}^2$. This layer does not noticeably affect the electrical and optical properties of GaMnAs and can be quite easily removed in a hydrochloric acid solution [1,2]. We can assume that for the said conditions of implantation and PLA a layer, where the manganese atoms are in the Mn_{Ga} state, is located at depths from 50 to 125 nm from the original surface, since it is at these depths that predominance of As over Ga is recorded to be within 2–3 at.% by the PLA method. The concentration of the Mn atoms in sites of the gallium sublattice is also estimated to be like this.

Secondly, the Curie temperature (T_C) for the samples produced at the manganese ions implantation energy of 180 kV, the dose of $5 \cdot 10^{16}\,\text{cm}^{-2}$ and when $P = 300\,\text{mJ/cm}^2$ was 120 K [12]. For the GaMnAs sample produced in the present study when $U = 80\,\text{kV}$, $D_i = 5 \cdot 10^{16}\,\text{cm}^{-2}$, $P = 400\,\text{mJ/cm}^2$, the Curie temperature is also 120 K (Fig. 9). Note that T_C almost does not depend on the energy of the ions Mn^+ within the range 40–200 keV for monoenergetic implantation [20]. At the same time, for the ions energy of 180 keV we observed a heavy dependence on the implantation dose: already for $D_i = 3 \cdot 10^{16}\,\text{cm}^{-2}$ the value of T_C is reduced to 60 K [12]. The dose dependence has also been observed in the present study, but it is significantly weaker: for the doses $3 \cdot 10^{16}$ and $2 \cdot 10^{16}\,\text{cm}^{-2}$ the value of the Curie temperature was 110 and 100 K, respectively (Fig. 9).

Thirdly, the nature of the magnetic-field dependences of Hall resistance (Fig. 8), magnetoresistance (Fig. 10) and their changes when varying the temperature generally corresponds to the behavior that has been previously observed for the samples produced by monoenergetic implantations of the ions Mn^+ [12].

Fourthly, after PLA, the X-ray diffraction studies of gallium arsenide irradiated with the Mn ions (Fig. 3) have shown that the curves noticeably differ from the diffraction patterns of the sample produced with the energy of 180 keV [12]. In particular, for the irradiated sample, after laser annealing ($300\,\text{mJ/cm}^2$) the study [12] includes a visible peak from the deformed GaMnAs layer to the left of the peak of the GaAs substrate, whereas after similar annealing the present study includes just asymmetrical widening of the base peak to the left, while after PLA with $P = 400\,\text{mJ/cm}^2$ this place originates thickness oscillations (Fig. 3). Another difference is a shape of the curve to the

right of the substrate peak ($2\Theta > 66.05^\circ$): for the sample irradiated at 180 keV, PLA was followed by appearance of a wide peak observed as a shoulder when $2\Theta \sim 66.6^\circ$ [12], whereas when $U = 80$ kV, $D_i = 5 \cdot 10^{16}$ cm^{-2} the diffraction pattern exhibits no such peak. The narrow peak when $2\Theta = 66.12^\circ$ is a known artefact of shooting. It is clear that defect structures of the comparable samples differ, although the galvanomagnetic properties are similar. We just note that the coercive fields obtained from magnetic-field measurements of the Hall effect differ for the samples with the same implantation dose ($3 \cdot 10^{16}$ cm^{-2}) and the same PLA energy (300 mJ/cm^2): 910 Oe for implantation with $E_i = 180$ keV [12] and 505 Oe for $U = 80$ kV (see the present study, Fig. 9). The said values correspond to the measurement temperature of 10 K. Most likely, it is also related to differences of the defect structure of the comparable samples.

Fifthly, the RS investigation revealed similar predominance of the coupled phonon-plasmon mode in the spectra both for the samples irradiated with the ions Mn^+ with the energy of 180 keV (at 261.5 cm^{-1}) [12] and for the samples with $U = 80$ kV studied herein, for which the position of the CPPM peak correlates with the changes of the hole concentration p_v and is shifted from 265 to 261 cm^{-1} with the increase of the implantation dose (Fig. 6, *b*).

Conclusion

It is shown in the study that using the vacuum-arc ion accelerator (in particular, the „Raduga-3M" accelerator) makes it possible to successfully implant manganese into GaAs in order to form the GaMnAs ferromagnetic semiconductor when applying the well-known diagram „ion implantation and subsequent pulsed laser annealing". With selecting only two factors as the technology parameters: the dose of the Mn ions within $2-5 \cdot 10^{16}$ cm^{-2} and the laser annealing energy density of about 300 mJ/cm^2 — we have produced the ferromagnetic semiconductor layers with the Curie temperature within $100-120$ K both for accelerating voltage of 80 kV and for 30 kV as well. At the room temperature of the measurements, the produced layers have optical (the coupled phonon-plasmon mode prevails in the RS spectrum) and electrical (mobility of carriers is about 5 cm^2/(V·s)) properties that are similar to the properties of the GaMnAs layers made using monoenergetic implantation and typical for the heavily-doped (with the concentration of up to $3 \cdot 10^{20}$ cm^{-3}) semiconductors of the *p*-type of conductivity. With the decrease of the measurement temperature below T_C, the Hall effect becomes anomalous, magnetoresistance is generally negative when there are portions of anisotropic MR, and the magnetic-field dependence of Hall resistance exhibits the hysteresis loop. The coercive field is the highest at 10 K, its value increases with an increase of the dose of the Mn ions within the above-said dose interval, while with an increase of the measurement temperature it monotonically decreases to the Curie temperature. Generally, the galvanomagnetic properties of the ferromagnetic semiconductor GaMnAs layers made using the vacuum-arc accelerator almost coincide with the properties of the GaMnAs layers, which are obtained during monoenergetic implantation. However, monoenergetic implantation may exhibit the heavy dependence of the Curie temperature on the dose of the implanted ions. For the method of implantation, which is used herein, we observe an insignificant dose dependence of the temperature of the ferromagnetic-paramagnetic phase transition.

Funding

The study is supported by the Russian Science Foundation (grant No. 24-72-00047).

Conflict of interest

The authors declare that they have no conflict of interest.

References

[1] S. Zhou. J. Phys. D: Appl. Phys., **48**, 263001 (2015). DOI: 10.1088/0022-3727/48/26/263001
[2] M.A. Scarpulla, R. Farshchi, P.R. Stone, R.V. Chopdekar, K.M. Yu, Y. Suzuki, O.D. Dubon. J. Appl. Phys., **103**, 073913 (2008). DOI: 10.1063/1.2890411
[3] C. Xu, M. Wang, X. Zhang, Y. Yuan, S. Zhou. Nuclear Inst. Methods Phys. Res. B, **442**, 31 (2019). DOI: 10.1016/j.nimb.2018.12.049
[4] Y. Yuan, Y. Xie, N. Yuan, M. Wang, R. Heller, U. Kentsch, T. Zhai, X. Wang. Materials, **14**, 4138 (2021). DOI: 10.3390/ma14154138
[5] M. Tian, Q. Yang, Y. Yuan, U. Kentsch, K. Liu, M. Tang, Z. Xie, L. Li, M. Wang. Results Phys., **58**, 107508 (2024). DOI: 10.1016/j.rinp.2024.107508
[6] Yu.A. Danilov, H. Boudinov, O.V. Vikhrova, A.V. Zdoroveishchev, A.V. Kudrin, S.A. Pavlov, A.E. Parafin, E.A. Pitirimova, R.R. Yakubov. FTT, **58** (11), 2140 (2016) (in Russian). DOI: 10.21883/ftt.2016.11.43727.4k
[7] I.G. Brown. Rev. Sci. Instrum., **65** (10), 3061 (1994). DOI: 10.1063/1.1144756
[8] A.I. Ryabchikov, N.M. Arsubov, N.A. Vasilyiev, S.V. Dektyarev. Nuclear Instr. Meth. Phys. Res. B, **59−60**, 124 (1991). DOI: 10.1016/0168-583X(91)95190-O
[9] A.I. Ryabchikov, S.V. Dektjarev, I.B. Stepanov. Rev. Sci. Instrum., **65** (10), 3126 (1994). DOI: 10.1063/1.1144766
[10] I.L. Kalentyeva, O.V. Vikhrova, Yu.A. Danilov, M.V. Dorokhin, B.N. Zvonkov, Yu.M. Kuznetsv, A.V. Kudrin, D.V. Khomitsky, A.E. Parafin, P.A. Yunin, D.V. Danilov. J. Magn. Magn. Mater., **556**, 169360 (2022).
[11] Electronic source. Available at: www.SRIM.org
[12] Yu.A. Danilov, Yu.A. Agafonov, V.I. Bachurin, V.A. Bykov, O.V. Vikhrova, V.I. Zinenko, I.L. Kalent'eva, A.V. Kudrin, A.V. Nezhdanov, A.E. Parafin, S.G. Simakin, P.A. Yunin, A.A. Yakovleva. FTT, **65** (12), 2230 (2023) (in Russian). DOI: 10.61011/FTT.2023.12.56767.230
[13] Kh. Rissel, I. Ruge. *Ionnaya implantatsiya* (Nauka, M.,1983), 360 s. (in Russian).

[14] A.V. Boryakov, S.I. Surodin, R.N. Kryukov, D.E. Nikolichev, S.Yu. Zubkov. J. Electron Spect. Related Phenomena, **229**, 132 (2018).
[15] Yu.I. Ukhanov. *Opticheskie svoistva poluprovodnikov* (Nauka, M., 1977), 367 s. (in Russian).
[16] P.Yu.M. Kardona. *Osnovy fiziki poluprovodnikov* (Fizmatlit, M., 2002), 560 s. (in Russian).
[17] W. Limmer, M. Glunk, S. Mascheck, A. Koeder, D. Klarer, W. Schoch, K. Thonke, R. Sauer, A. Waag. Phys. Rev. B, **66**, 205209 (2002). DOI: 10.1103/PhysRevB.66.205209
[18] M.J. Seong, S.H. Chun, H.M. Cheong, N. Samarth, A. Mascarenhas. Phys. Rev. B, **66**, 033202 (2002). DOI: 10.1103/PhysRevB.66.033202
[19] N.G. Galkin, S.V. Vavanova, K.N. Galkin, R.I. Batalov, R.M. Bayazitov, V.I. Nuzhdin. ZhTF, **83** (1), 99 (2013) (in Russian).
[20] Yu.A. Danilov, V.A. Bykov, O.V. Vikhrova, D.A. Zdoroveishchev, I.L. Kalent'eva, R.N. Kryukov, A.E. Parafin, Yu.A. Agafonov, V.I. Zinenko, R.I. Batalov, V.F. Valeev, V.I. Nuzhdin. FTT, **66** (6), 871 (2024) (in Russian). DOI: 10.61011/FTT.2024.06.58239.24HH

Translated by M.Shevelev